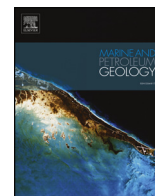




ELSEVIER

Contents lists available at ScienceDirect

Marine and Petroleum Geology

journal homepage: www.elsevier.com/locate/marpetgeo

Research paper

Fracture mechanical properties of carbonate and evaporite caprocks in Sichuan Basin, China with implications for reservoir seal integrity

Zonghu Liao^{a,b}, Mengni Wu^b, Xiaofeng Chen^{c,*}, Huayao Zou^{a,b}^a State Key Laboratory of Petroleum Resources and Prospecting, China University of Petroleum (Beijing), Beijing, 102249, China^b College of Geosciences, China University of Petroleum (Beijing), Beijing, 102249, China^c Department of Geology and Geophysics, Texas A&M University, College Station, TX, 77845, USA

ARTICLE INFO

Keywords:

Subcritical fracture
Caprock integrity
Carbonate
Anhydrite
Mineral dissolution

ABSTRACT

Fracture development in reservoir rocks enhances the flow and transport properties of the petroleum system, yet fracture in caprocks can significantly risk reservoir seal integrity. Over geological time scales, the slow, subcritical fracture propagation can contribute considerably to the fracture system development, especially under reactive fluid environments during petroleum migration and accumulation. Using the double torsion technique, we measure the subcritical fracture growth properties of carbonate and anhydrite caprock core samples in Sichuan Basin, China, under different environments of ambient air, de-ionized water, and formation water. Experimental results show that the aqueous fluids significantly promote subcritical fracture growth: (1) compared to ambient air, the presence of aqueous fluids dramatically reduces both the fracture toughness (K_{IC}) and subcritical fracture growth index (SCI) of the caprocks; (2) the K_{IC} reduction is more prominent for the anhydrite (50%) caprock than the carbonate (30%) caprock, which suggest that mineral solubility is responsible for the fluid-weakening effect; (3) a systematic change of SCI with varying fluid conditions is observed: SCI is the largest in air, smallest in formation water, and intermediate in de-ionized water. Microstructural analysis suggests a predominantly opening mode for both the natural fractures and induced fractures during fracture mechanical testing. Our results further demonstrate that subcritical fracture growth process is also strongly related to rock composition and stress conditions. These observations provide insights into the mechanisms controlling fracture growth in carbonate and evaporite caprocks, which could extend to brittle failure and fluid-rock interactions occurring during the seismic cycle in the upper crust.

1. Introduction

Caprock is a crucial component in subsurface storage reservoirs. For effective trapping of oil and gas in petroleum systems, an effective caprock should meet a suite of requirements in its petro-physical and rock mechanical properties. For intact caprocks, low permeability membrane seals in the pore throats are essential for providing permeability barrier to trap the fluid from migrating upward through sealing intervals (e.g., Downey, 1984; Watts, 1987). However, rocks frequently fail by fracturing and faulting under subsurface stress and temperature conditions which can compromise caprock sealing performance. For example, unsealed faults are frequently identified in petroleum exploration practices as examples of seal failure (Allan, 1989; Fisher et al., 2001; Finkbeiner et al., 2001; Hao et al., 2015). For sealed faults, risk assessment for seal failure is also necessary because of the potential for fault reactivation (Smith, 1966; Yielding et al., 1997; Fulljames et al.,

1997) within the critically stressed crust (Zoback, 2010). Fractures within tight formations can provide fracture porosity for storage and pathway for fluid migration, which significantly enhances the storage and flow properties of the host rocks (Olson et al., 2009; Cipolla et al., 2010). In contrast, fracture growth in caprocks can be a detrimental process that compromises the caprock integrity (Ingram and Urai, 1999; Cosgrove, 2001; Tingay et al., 2009; Hao et al., 2015). As a result, the overall caprock sealing efficiency is related to both how impermeable the caprocks are and how well the caprocks can withstand failure by faulting and fracturing under in-situ stress, temperature, and fluid conditions.

Rock failure characteristics are commonly investigated experimentally through rock mechanical and fracture mechanical testing under relevant stress conditions (e.g., Lee et al., 2015; Zhang et al., 2017), different fluid chemical environments (e.g., Erguler and Ulusay, 2009; Nara et al., 2012; Chen et al., 2019a), and variable temperatures (e.g.,

* Corresponding author.

E-mail addresses: xfchen0515@gmail.com, xiaofengchen@tamu.edu (X. Chen).<https://doi.org/10.1016/j.marpetgeo.2020.104468>

Received 22 November 2019; Received in revised form 18 April 2020; Accepted 14 May 2020

Available online 17 May 2020

0264-8172/ © 2020 Elsevier Ltd. All rights reserved.

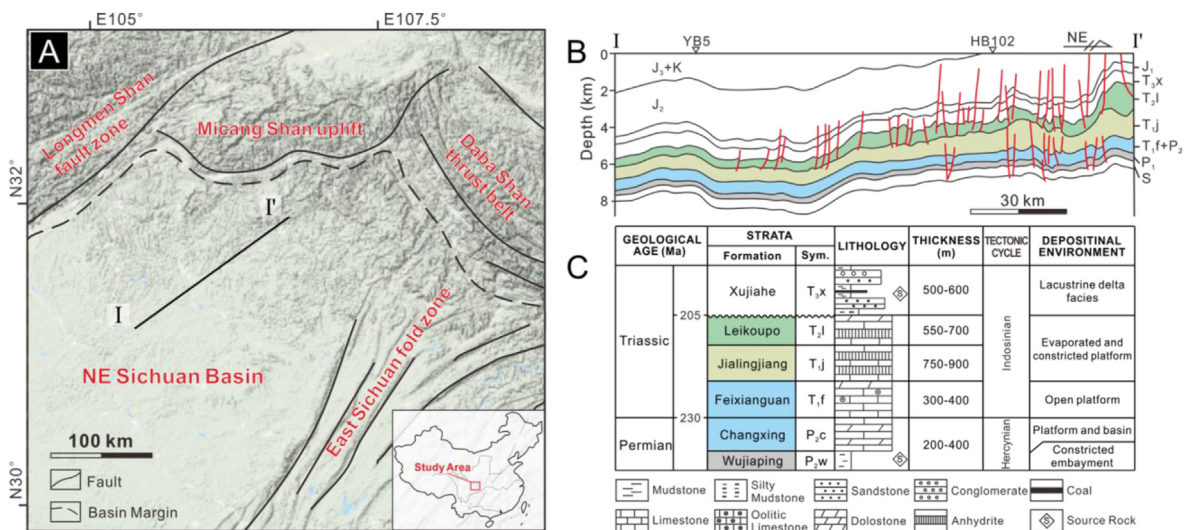


Fig. 1. Geologic setting of the study area. (A) Major structures are bounding the NE Sichuan Basin. Inset marks the location of the Sichuan Basin (green shade) and the mapped area in A (square). (B) Stratigraphic units crossing the blue line in (A) constructed from well-logs and seismic data. Major faults marked in red. (C) Typical stratigraphic columns for the present petroleum system (adapted from Li et al., 2015). (For interpretation of the references to color in this figure legend, the reader is referred to the Web version of this article.)

Handin et al., 1967; Meredith and Atkinson, 1985; Atkinson and Meredith, 1987). Rock mechanics testing can determine rock strength, failure modes, failure envelope, and failure microstructures, along with other rock physical properties (Sone and Zoback, 2013; Chen et al., 2017). Fracture mechanical testing, on the other hand, explores the fracture growth properties within the rocks. For instance, fracture toughness, or K_{IC} with the unit of $MPa\sqrt{m}$, is a measure of the ability for materials to resist fracture (Anderson, 2005). When the stress state near a fracture tip, named stress intensity factor K , which is a function of applied stress and fracture geometry, approaches the fracture toughness of the material, critical fracture propagation is expected, e.g., in dynamic rupture propagation (Reches and Lockner, 1994) and hydraulic fracturing (Cosgrove, 2001; Tingay et al., 2009) processes. Fractures can also propagate subcritically when $K < K_{IC}$, by chemically assisted processes such as stress corrosion (Atkinson, 1982, 1984) and mineral dissolution (Major et al., 2018). Subcritical fracture growth is related to the long-term, environmentally assisted processes such as joint system development, static fatigue, and creep deformation (Olson, 1993).

The recent interest in unconventional petroleum resource development, subsurface waste storage, and hydrothermal systems resulted in increased interest in geomechanical properties in tight formations (e.g., Meléndez-Martínez and Schmitt, 2016; Major et al., 2018; Chen et al., 2019a, 2019b; Callahan et al., 2019). Carbonates generally deform brittly under upper crustal conditions, but they can also have ductile failure under elevated temperature and confining pressure (Handin et al., 1963) or assisted by pore fluids (Renner and Rummel, 1996) associated with considerable porosity, small grain size, and the presence of clay minerals (Chen et al., 2019b). Having similar evaporative origin, halite, gypsum, and anhydrite are often thought of as ideal caprocks due to their dominant ductile flow characteristic even under shallow depth stress and temperature conditions (Handin and Hager, 1958; Chester, 1988; Shimamoto, 1986; Fu et al., 2016) and their low permeability and porosity. Fracture toughness and brittleness measurements are routinely conducted to guide hydraulic fracturing operations (e.g., Jin et al., 2014a). As a result, a large amount of literature reported fracture toughness values in tight formations such as shales (Swanson, 1984; Chen et al., 2017, 2019a, 2019b) and tight carbonates (Brantut et al., 2013; Piane et al., 2017). However, there are few studies on slow subcritical fracture growth properties in tight formations, especially for rock salts under reactive fluids.

Previous studies show that fluid pH and cation concentration impact

subcritical fracture growth (Billi et al., 2003; Rostom et al., 2013). However, no previous study focused on the fracture growth properties in rock salts, primarily due to the abovementioned strong flow properties of these evaporites, which renders brittle deformation features unlikely to occur or quickly healed/sealed during ductile flow. Despite their strong potential to withstand brittle deformation, rock salts are vulnerable under fluids due to their much more significant solubility than carbonates and silicates. Since mineral dissolution is thought to be an effective mechanism of subcritical fracture growth in carbonates (Bergsaker et al., 2016; Chen et al., 2019b) and silicates (Atkinson and Meredith, 1981), it is reasonable to assume that gypsum/anhydrite dissolution can also be a significant contributing factor for subcritical fracture growth. In addition, the massive swelling potential of anhydrite-gypsum transformation could make initial cracks a contributing factor for fracture system development (Bildstein et al., 2001; Machel, 2001; Fu et al., 2016). For petroleum systems, subcritical fracture growth may control brittle deformation processes at tectonic loading rates, at slow pore pressure buildup during burial and maturation of organic-rich sediments, and at the interfaces of changing fluid composition during migration of hydrocarbons (Chen et al., 2017). Therefore, assessment of the interaction between fluid and fractures in hydrocarbon systems is necessary.

In this study, we focus on the fracture characteristics of the carbonate and anhydrite caprocks, specifically in a deep gas reservoir in Sichuan Basin, China. We conduct double torsion fracture mechanical testing on core caprock samples of carbonates and anhydrite under various fluid chemical environments of air, de-ionized water, and formation water to get fracture growth parameters of fracture toughness, subcritical fracture growth index (SCI) and stress intensity vs fracture velocity curves. We also compare the microstructures between natural fractures and those formed during the fracture mechanics testing. The controlling mechanisms for fracture development in marine evaporites under subsurface conditions are discussed, and the general implication for caprock failure in deep gas reservoirs is addressed.

2. Geologic setting

The Sichuan Basin is the largest natural gas-rich basin in Southwest China (Dai et al., 2014; Li et al., 2015). Northeast Sichuan Basin is located at the northern margin of the Yangtze plate, surrounded by the Micangshan uplift in the north, Dabashan thrust belt in the northeast,

and East Sichuan fold belt in the east (Fig. 1A). The major petroleum systems are distributed in three sub-divisions: the Tongnanba anticline in Dabashan forebulge, the Yuanba area in the slope of the Micangshan uplift, and the Xuanhan-Daxian area in the edge of East Sichuan fold belt (Fig. 1A). Two large deposition stages associated with the petroleum systems are identified in the Northeast Sichuan Basin: marine carbonate deposition from Permian to Middle Triassic periods and terrestrial clastic rock deposition from Late Triassic to Middle Paleogene (Fig. 1B and C).

This study focuses on the petroleum systems in marine strata from Permian to Middle Triassic periods. The source rocks are organic-rich shale and dark marl in the Permian Wujiaping Formation (P_{2w}). The main reservoir rocks are the striped reef-bank dolostone along the platform margin in the Upper Permian Changxing Formation (P_{2c}) and the shallow shoal oolitic dolostone and limestone in the Lower Triassic Feixianguan Formation (T_{1f}). The carbonates (P_{2c}, T_{1f}) underwent intense dolomitization, dissolution and fracturing, which altogether made them high quality fractured dolomite reservoir. However, the tight and impermeable carbonates made them direct caprocks overlaying the carbonate reservoir rocks. The dense limestone usually formed at platform slopes and outer shelf overlaying porous shoal facies reservoir rocks (Jin, 2012; Jin et al., 2014b). From Late Feixianguan Age, the open platforms gradually transitioned to restricted platforms and eventually to evaporative platforms as sea level regressed. Evaporite layers (mainly anhydrite) started to deposit, interbedded with mud-grade carbonate rocks in the Upper Feixianguan Formation. Thick anhydrite, gypsum, and halite rocks compose most of the Jialingjiang Formation (T_{2j}). Anhydrite interbeds with micritic dolostone in Leikoupo Formation (T_{2l}). These evaporites gradually thickened from the edge toward the center of the basin (NE to SW) and covered nearly the whole Northeast Sichuan Basin with an average thickness of over 350 m (Wei et al., 2011; Zhang et al., 2012). Seismic and logging evidence confirmed that major faults died out in these evaporite-bearing formations (Fig. 1B), suggesting that the evaporites are ideal regional caprocks for the underlying petroleum resources (Ma et al., 2008).

Fractures play an essential role in the current petroleum system. On the one hand, fracture network within the carbonate rocks improves the reservoir storage capacity (Ma et al., 2007; Guo, 2018). On the other hand, field exploration data suggested that whether fractures can develop within the dense impermeable carbonate caprocks overlaying the reservoir rocks is critical for caprock sealing efficiency. For instance, fractures developed in the tight, fold-modified Middle-Upper Feixianguan Formation, making it a fractured reservoir. While in the Yuanba area, the same Formation served as locally direct caprock due to the lack of fractures. The indirect caprocks of anhydrite and gypsum did not show clear evidence of seal failure from seismic data (Fig. 2B), but there is a need to evaluate the effect of fluids on compromising the

integrity of these evaporites as the likelihood of evaporite caprock failure is high. For instance, geochemical evidence (Wang et al., 2013) show clear evidence of marine gas migrating through the evaporite formations to charge the Xujiahe reservoir above the evaporite (Fig. 2C).

3. Materials and methods

3.1. Materials

The materials used are core samples from four wells within three formations, with the depth range of 4142–6705 m (13,589–21,998 ft) below ground in NE Sichuan Basin (Table 1). Powder X-ray diffraction (XRD) analysis determines bulk mineralogy of the four samples (Table 1). The fragmented core samples were first crushed and pulverized. The sieved portion was then ground in a micronizing mill for 5 min with ethanol. The slurry was then oven-dried at 70 °C (well below the gypsum-anhydrite transition temperature of 200 °C at normal atmospheric condition as in Deer et al. (1992)). The dry powder was then mounted on the glass sample holder and inserted into the Rigaku Ultima IV diffractometer for XRD analysis using Cu K α radiation, 2–70° 2 θ scan range, and 0.02° step size. JADE software was used for peak identification. T_{1j} and T_{2l} are anhydrite-bearing regional caprocks. T_{1j} from well HB102 is composed of predominantly anhydrite, while T_{2l} from well YB204 is dolomitic anhydrite. T_{1f} is a carbonate-rich direct caprock. T_{1f} from Well YB5 is limestone with 94% calcite, while T_{1f} from well MB2 is muddy as it has less calcite but contains small amount of dolomite, clay, and pyrite.

The recovered core samples and the thin-section images display the general appearance and texture of the caprocks. T_{1j} from well HB102 has fine planer lamination (Fig. 2A), with tortuously striped anhydrite crystals as large as hundreds of μ m tightly aligned with neighboring grains (Fig. 2E). T_{2l} from well YB204 shows wavy and thicker laminations, with the dark dolomitic layers interbedded with the lighter anhydrite layers (Fig. 2B). The thin-section image reveals the interconnected anhydrite crystals and the muddy textured dolostone (Fig. 2F). T_{1f} from well YB5 is homogeneous with fine lamination (Fig. 2C), and a tight microcrystal calcite matrix as displayed in the thin-section image (Fig. 2G). T_{1f} from well MB2 has more impurities as indicated by the wavy and lighter bands in the core sample (Fig. 2D) and the dark spots in the thin section image (Fig. 2H). Except for a few cracks along bedding interfaces, all three formations display very few natural fractures in the core samples. All formations have a tight matrix with few/no visible pore spaces in the thin sections.

The basic physical properties of these rocks are compiled in Table 2. Porosity was calculated based on mineralogy data from XRD analysis. Dynamic Young's modulus and Poisson's ratio were calculated using

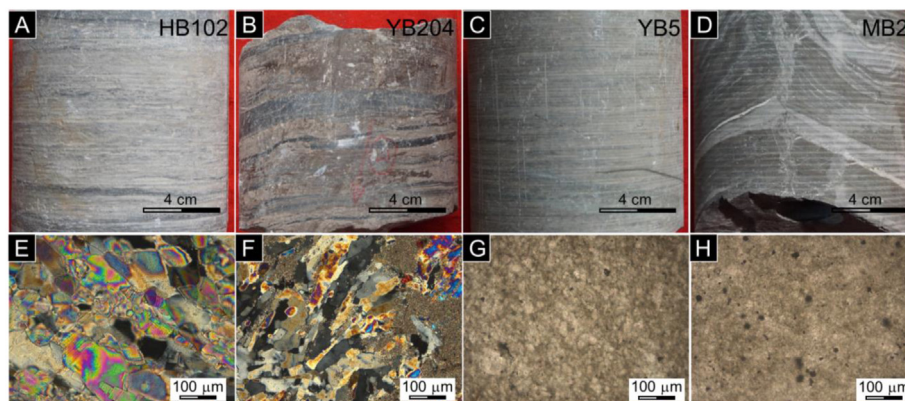


Fig. 2. Recovered core samples (A–D) from the caprocks of deep gas reservoirs in NE Sichuan Basin and their thin-section images (E–H). Thin-section planes were parallel to bedding and were imaged under cross-polarized light (E, F) and plane-polarized light (G, H). See the text for descriptions.

Table 1
Mineralogy of the caprock core samples determined from XRD analysis.

Well	Formation	Depth (m)	Mineral type (%) ^a					
			anhydrite	gypsum	calcite	dolomite	quartz	others
HB102	T _{1j}	4705–4712	98	–	–	–	2	–
YB204	T _{2l}	4891–4893	62	4	–	30	4	–
YB5	T _{1f}	6703–6705	–	–	94	–	6	–
MB2	T _{1f}	4142–4145	–	–	70	11	6	13 ^b

^a Mineral composition is in weight percent.

^b 12% chlorite, and 1% pyrite.

measured sample density and ultrasonic P-wave and S-wave velocities at zero confining pressure under elastic isotropic assumption. Wave speeds were transmitted using core plugs with the axial direction perpendicular to bedding. Static Young's modulus and Poisson's ratio are derived from unconfined compressive tests with compression normal to bedding. The static Poisson's ratio values were used for later stress intensity factor calculations. Equations for fracture propagation in elastic anisotropic materials can be found in [Nara and Kaneko \(2006\)](#).

3.2. Experimental methods

A double torsion (DT) test is suitable to measure fracture behavior, especially for investigating subcritical fracture growth under reactive fluids ([Atkinson, 1984](#); [Chen et al., 2019a](#)). The loading configuration consists of a symmetric four-point support at the corners of a rectangular plate with loading applied from the two points at the top edge of the plate ([Fig. 3A](#)). The stress intensity factor K_I and fracture velocity are calculated as ([Williams and Evans, 1973](#)):

$$K_I = PW_m \left[\frac{3(1 + \nu)}{Wd^3d_n\psi} \right]^{1/2} \quad (1)$$

$$V = -\phi \frac{P_0 a_0}{P^2} \frac{dP}{dt} \quad (2)$$

In equation (1), P is the applied load, W_m is bending moment arm, W is specimen width, d is specimen thickness, d_n is the reduced specimen thickness in the groove ([Fig. 3A](#)), ν is Poisson's ratio, and ψ is the thickness correction factor expressed as ([Fuller, 1979](#)): $\psi = 1 - 1.26(d/W) + 2.4(d/W)\exp(-\pi W/2d)$. In equation (2), ϕ is a geometric correction factor taking into account the curved crack front, P_0 and a_0 are the load and crack length at the beginning of the relaxation period, respectively. We chose $\phi = 0.2$, as suggested by [Williams and Evans \(1973\)](#) and a constant $a_0 = 13$ mm ([Chen et al., 2017](#)). With both K_I and V , the K - V curves can be constructed and the power law fitting of the K - V curves yields the SCI as ([Atkinson, 1984](#); [Brantut et al., 2013](#)): $V = AK_I^n$, where A is an experimental constant, n is the SCI measuring the susceptibility of subcritical fracture growth for materials in the specific environments.

Core samples were sliced parallel to bedding and smoothed to rectangular wafers of 75 mm by 25 mm by 2 mm. Rectangular fracture guiding grooves of 0.4 mm in depth and 1 mm in width were cut on one side of each specimen ([Fig. 3B](#)). The specimens were tested in three

conditions: ambient air (at room humidity of ~50%), de-ionized (DI) water, and formation water at room temperature of ~20 °C. The specimen wafers were soaked in relative fluids of DI water and formation water for 24 h before the DT tests to ensure complete fluid saturation. Laboratory formation water composition was based on ion chromatography results of formation water at relevant layers ([Table 3](#)). Intact wafers were first pre-cracked under a specific environment under a slow loading rate of 0.05 mm/s to introduce the starting fracture ([Holder et al., 2001](#); [Chen et al., 2017](#)). The pre-cracked specimens were loaded at 0.5 mm/s to load level of approximately 80%–90% K_{IC} . The load point was then held still to allow load relaxation for ~10 min. In a typical load relaxation test, ~4 load-relaxation cycles can be applied before the fracture propagates to the end of the specimen. The maximum load was used to calculate K_{IC} (termed K_{IC}^*) using Equation (1). Due to sample inhomogeneity, such as existing fractures, layering contrast, and uneven crystal domains, some fractures can propagate deviating from the central axis, which was categorized as failed tests and were not used for further analysis. The DT test apparatus ([Fig. 3D](#)) consists of a stepper motor (Automation direct STP-MTR-23079) for displacement control, a S-beam load cell (Omega LCCD-50) with maximum range of ~50 lbs (23 kg) for load measurement, a non-contact linear displacement sensor (Omega LD701-5/10) for displacement measurement, and a National Instrument USB-6001 with Labview software for data acquisition under sampling rate of 5 Hz.

Original core samples were made into thin-section slides for microstructural observations. Thin-section slides containing natural fractures were further used for scanning electron microscopy (SEM) analysis. Fractures formed during DT tests were also preserved for SEM imaging of both fracture surfaces and fracture traces.

4. Results

4.1. Fracture mechanical behavior

An example of the K - V curves for the anhydrite caprock T_{1j} from well HB102 is displayed in [Fig. 4](#). Some general features of the K - V curves for all the caprock samples can be drawn. First, the K - V curves generally follow the empirical power-law relation under all conditions tested, as represented by straight lines in the log-log space ([Fig. 4](#)). Second, the test condition strongly influences the K - V curves. From air towards formation water to DI water, the K - V curves shift toward lower stress intensity factor and higher fracture velocity (the upper-left corner

Table 2
Basic Physical properties of the caprocks tested.

Well	Density (g/cm ³)		Wave speed (m/s)		E (GPa)		Poisson's ratio		Φ (%)
	measured	calculated	P	S	dynamic	static	dynamic	static	
HB102	2.878	2.942	5052	2791	57.2	33.4	0.28	0.51	0.72
YB204	2.893	2.859	4937	2767	57.6	15.9	0.27	0.75	1.15
YB5	2.709	2.694	5544	2733	54.1	44.5	0.34	0.22	0.11
MB2	2.787	2.745	–	–	–	34.3	–	0.20	0.33

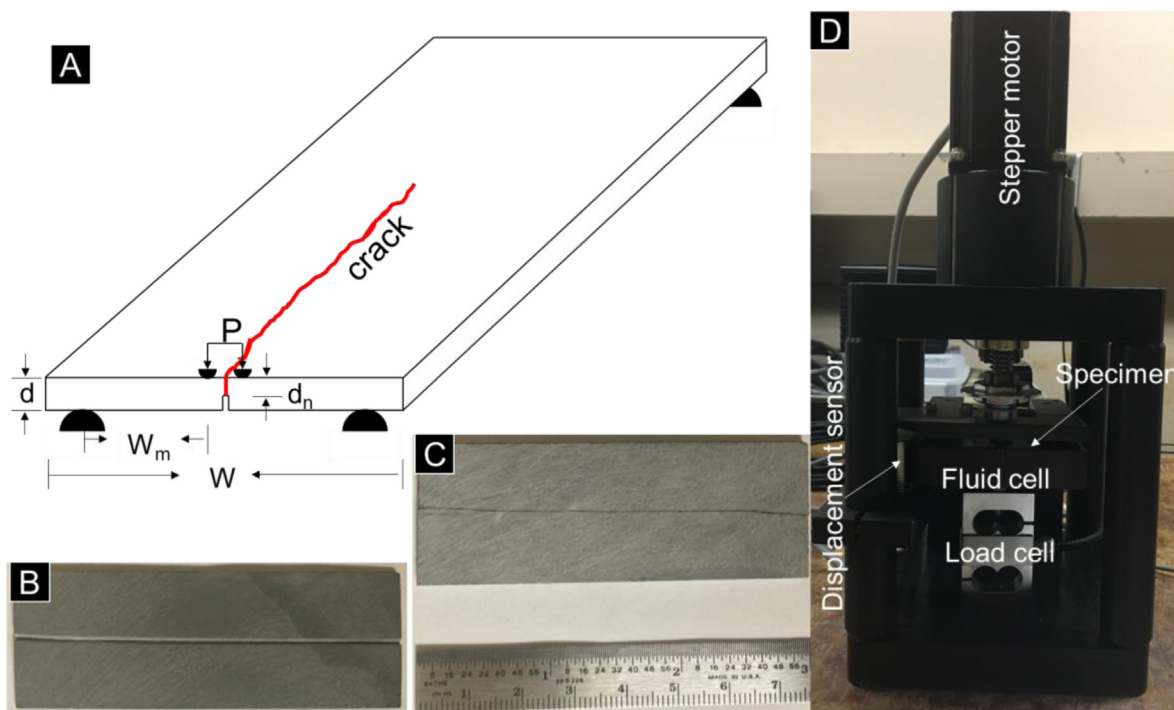


Fig. 3. The double torsion experimental method. (A) Loading configuration of the Double Torsion (DT) setup with useful specimen geometric parameters. (B) An intact MB2 specimen before DT testing with the fracture guiding groove facing upward. (C) A fractured YB5 specimen showing a fracture path along the central axis. (D) Experimental apparatus with main components.

Table 3
Formation water composition in mol/L.

Well	NaCl	KCl	CaCl ₂	MgCl ₂	Na ₂ SO ₄	Salinity (%)
HB102	0.76	–	0.56	0.13	–	104.99
YB204	1.278	0.196	0.423	0.364	–	141.21
YB5	0.508	–	0.258	0.029	0.014	57.29
MB2	0.783	0.135	–	–	0.115	67.27

in the K–V space). This shift marks an enhanced subcritical fracture growth: fractures propagate under lower K as the K–V curves shift leftward, and fractures move faster as the K–V curves shift upward. From the K–V curves, we derive the maximum stress intensity factor K_{IC}^* as an approximation to K_{IC} (Callahan et al., 2019), the specific K values at $V = 10^{-5}$ m/s (termed K_a) to measure the scatter of K under each test condition and the shift of K under different test conditions (Nara et al., 2012; Chen et al., 2017, 2019a, 2019b), and the SCI (slope of the K–V curve) to measure the rate-dependency of the stress intensity factor.

We now integrate the measured fracture mechanical properties of all samples. The synthesized K–V curves (Fig. 5A–D) were simplified based on the raw data (Fig. 4). Each curve was drawn based on its mean SCI (E–H) and mean K_a data (I–L), and then extended to the velocity range of 10^{-7} – 10^{-4} m/s. In ambient air, the anhydrite caprock from well HB102 has the largest fracture toughness, about $1.47 \text{ MPa m}^{1/2}$; while the other three caprocks are weaker, with K_{IC}^* around $1.2 \text{ MPa m}^{1/2}$. SCI spreads between 17 and 75. The systematic environmental effect on the shift of the K–V curves, SCI, K_{IC}^* , and K_a is maintained for all the samples. Compared to the air environment, DI water has the strongest effect on the shift of the K–V curve and the reduction of K_{IC}^* and K_a , while such weakening effect is smaller in formation water. The only exception is for the dolomitic anhydrite caprock from well YB204 (Fig. 5B and J), where both formation water and water have similar weakening effect on the shift of K–V curve, K_{IC}^* , and K_a . The introduction of fluids (water and formation water) induces

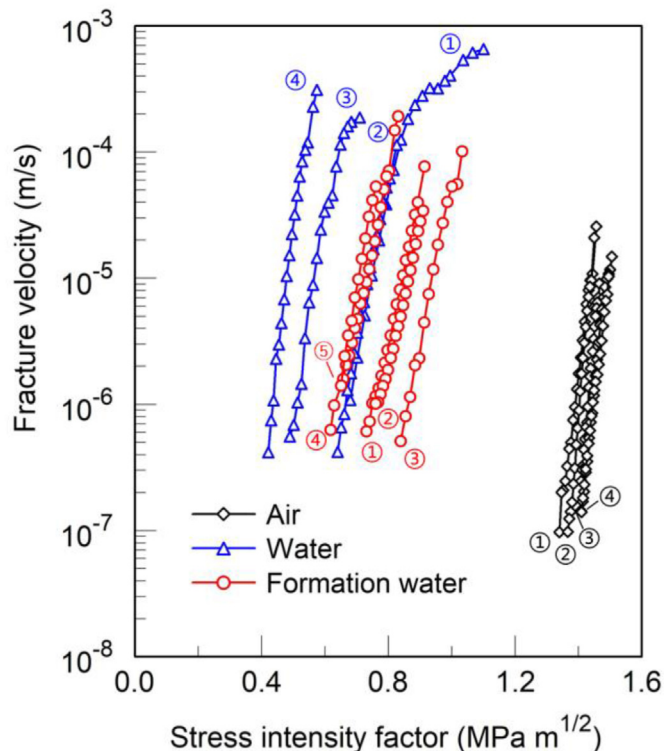


Fig. 4. K–V curves for the anhydrite caprock (HB102) tested under conditions of ambient air (black), De-ionized water (blue), and formation water (red). The load-relaxation sequences are also labeled for each fluid environment. (For interpretation of the references to color in this figure legend, the reader is referred to the Web version of this article.)

stronger shift of the K–V curves and stronger reduction of K_{IC}^* and K_a for the two anhydrite-rich caprocks (HB102 and YB204) than the

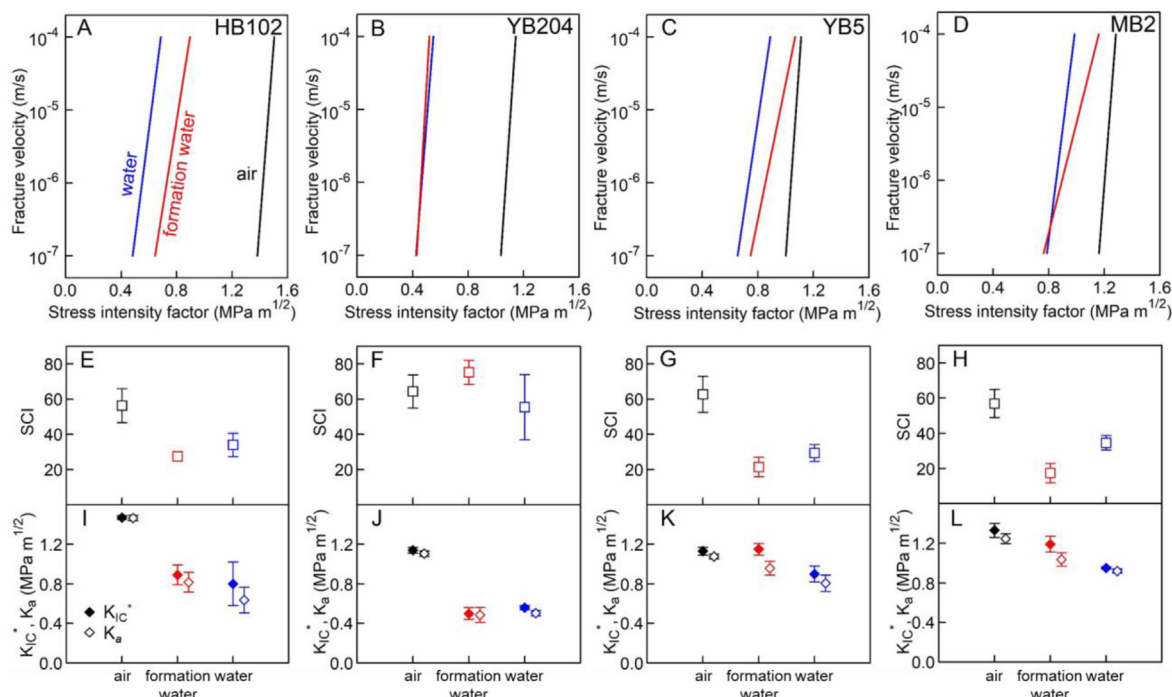


Fig. 5. Synthesis of the measured fracture mechanical parameters. A–D. Constructed K–V curves for the four wells under three test conditions of air (black), water (blue), and formation water (red). The color codes of black (air), blue (water), and red (formation water) apply to all figures here. E–H. Mean SCI with 1σ error bars. I–L. Mean fracture toughness (solid diamonds) and K_a (hollow diamonds) with 1σ error bars. K = Stress intensity factor, V = Fracture velocity, SCI = Subcritical fracture growth index. (For interpretation of the references to color in this figure legend, the reader is referred to the Web version of this article.)

carbonate caprocks (YB5 and MB2). For example, K_{IC}* and K_a reduced over 50% for HB102 and YB204 (Fig. 5I and J) under the two aqueous fluids of DI water and formation water, while such reduction is ~30% for the carbonate caprocks (Fig. 5K, L). A systematic change of the SCI is also observed (except YB204): SCI is the largest in air (~60), smallest in formation water (20–30), and intermediate in water (30–40).

4.2. Fracture microstructure

Fracture microstructures demonstrate both similarities and differences between natural fractures and fractures formed by DT tests. Only a few natural fractures are present in these caprock samples (Fig. 2A–D). We did not succeed in finding any natural fractures in the thin-section slides in the anhydrite caprock from well HB102. The example in Fig. 6A is a shale band impurity within the anhydrite matrix. YB204 exhibits natural fractures along the evaporite-carbonate boundary. These fractures extend into the carbonate matrix but terminate in the evaporite matrix (Fig. 6B). A thin natural fracture is captured in the carbonate caprock YB5, with the fracture space filled with calcite. The natural fracture example in MB2 has a bifurcation structure. This fracture was first filled with quartz (white crystals on the sidewall of the fracture), and then this fracture re-opened for additional calcite filling (black zone in the middle of the fracture) as confirmed by SEM energy dispersive spectrum analysis. Some of the natural fractures in MB2 also contain bitumen (not shown here).

Recognizing that natural fractures rarely exist in the anhydrite samples (Fig. 6A and B), the induced fractures propagate within the anhydrite matrix and can both cut across individual anhydrite grains and along the boundaries of two crystal domains (Fig. 6E and F). Because of the micritic texture, intergranular fracture propagation is dominant in the carbonate caprocks as displayed in Fig. 6G–H. The fracture paths can be either straight (Fig. 6E and H) or twisting (Fig. 6F and G). All these natural and induced fractures are predominantly opening mode, as can be identified from the matching shapes on fracture walls.

SEM images display fracture microstructures at finer scales. The fracture surfaces from anhydrite caprock from well HB102 expose abundant elongated anhydrite crystal grains (Fig. 7A–B). These grains have smooth surfaces, with only a few grains showing breakage surfaces (red arrows in Fig. 7A–B). The variation of test environments from air to water has a negligible effect on fracture surfaces for anhydrite caprock from well HB102. The anhydrite grains in the dolomitic anhydrite caprock from well YB204 are larger than those in HB102, with the fine-grained dolomite scattered between anhydrite domains (Fig. 7C–D). Sharp anhydrite grain edges are well preserved in the fracture surface formed in air (Fig. 7C), while the grain edges are less sharp in the fracture surface formed in formation water (Fig. 7D). Fracture surfaces in the two carbonate caprocks (YB5 and MB2) are similar in their fine-grain texture (Fig. 7E and H). Furthermore, fluid chemistry has similar effects in altering fracture surface morphology of these carbonate caprocks: the spotty surfaces formed in air (Fig. 7E and H) evolved to flatter surfaces formed in water (Fig. 7F and I), and to the smoothest fracture surfaces formed in formation water (Fig. 7G and J).

Fracture traces between the anhydrite and carbonate caprocks show contrasting features. On one hand, fractures show step-like traces in the anhydrite caprock (Fig. 7K), suggesting cleavage along preferred crystal planes as the main fracture growth process. The anhydrite fractures also have a wide damage zone around the fracture tip as seen by multiple bifurcated fracture traces (Fig. 7K). On the other hand, because of the fine-grain texture, the calcite grains have little influence on fracture traces along the carbonate caprock, and the damage zone is concentrated around the main fracture wall, as can be seen from the loose grains close to the fracture wall (Fig. 7L).

5. Discussion and implications

5.1. Comparison to other studies

For the carbonate caprocks (YB5, MB2), our measured fracture toughness data in air are ~1.2 MPa m^{1/2} (Fig. 5K, L), which is

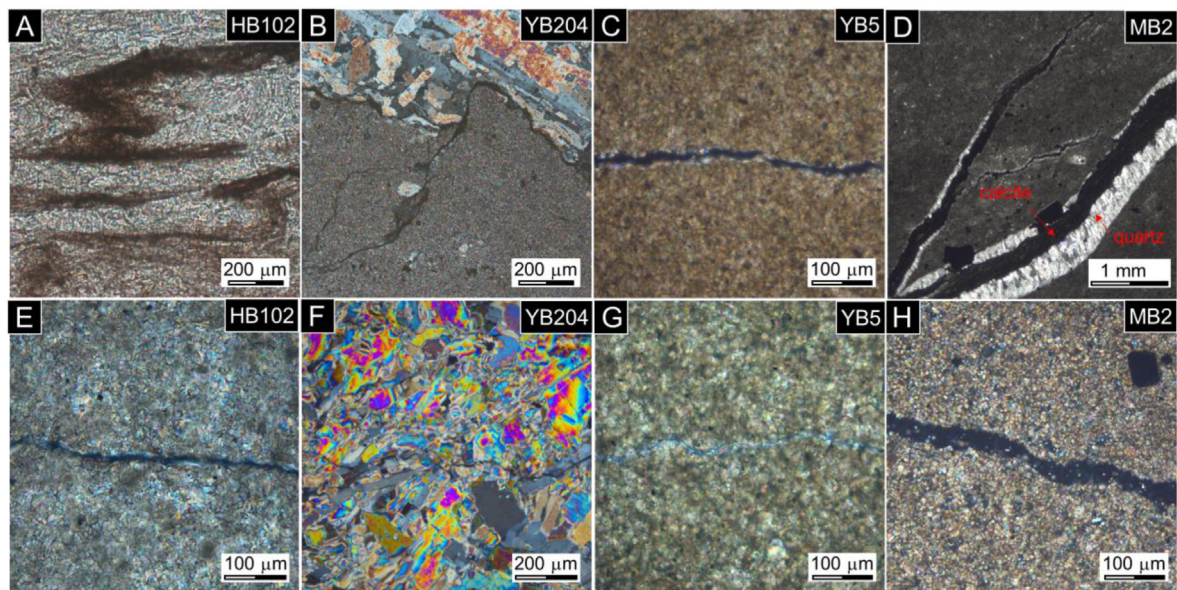


Fig. 6. Thin-section images of both natural fractures (A–D) and induced fractures during Double Torsion tests (E–H) under cross-polarized light. The quartz and calcite filling in the fracture in (D) were identified with energy dispersive spectrum analysis. See the text for details.

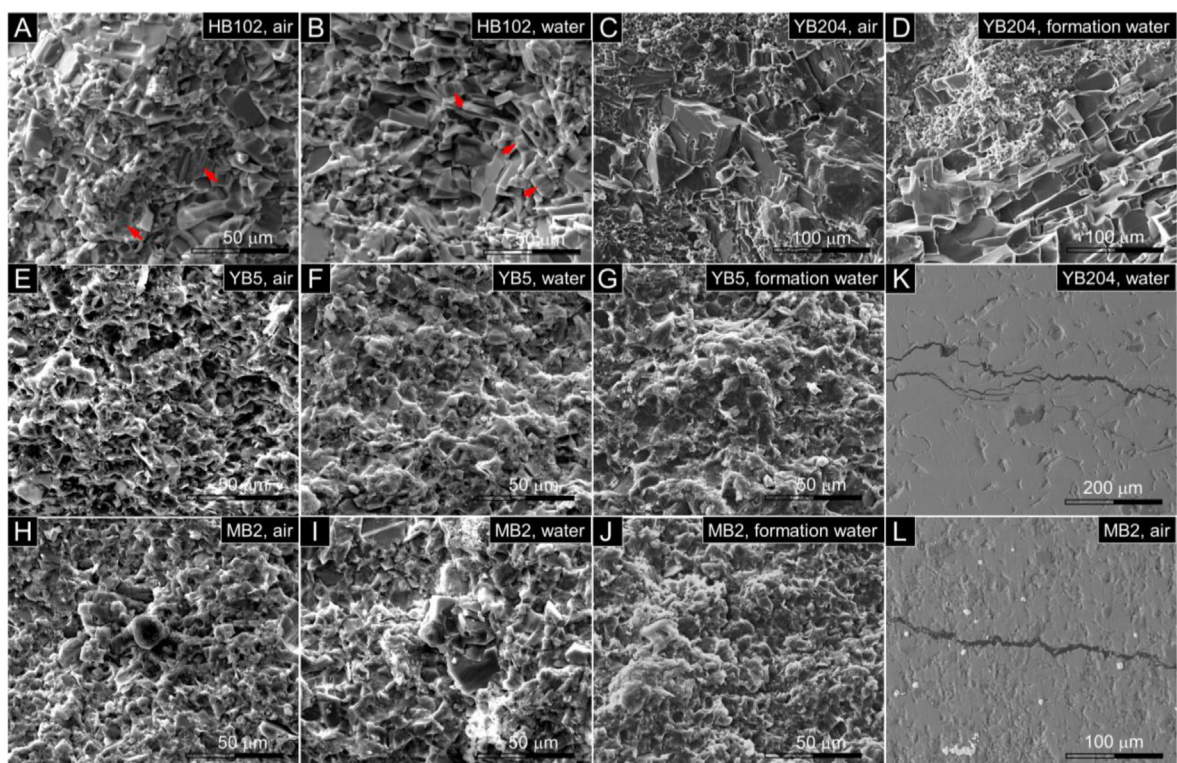


Fig. 7. SEM images of fracture surfaces (A–J) and fracture traces (K–L) formed during Double Torsion tests. See the text for details.

comparable to reported values for micritic limestone as summarized in Atkinson (1984) and in agreement with that for carbonate-rich Marcellus Shale in recent study by Chen et al. (2019a, 2019b). The reduction in fracture toughness, when exposed to water and formation water (Fig. 5K, L), is also in agreement with the well-documented water-weakening effect on rock strength and toughness (Mucci, 1983; Millero and Roy, 1997). We also observe a substantial reduction in SCI when exposed to water and DI water. SCI values in air are ~ 60 , comparable to those from the carbonate-rich Marcellus Shale (Chen et al., 2019b), and the lower SCI values of 20–40 for wet carbonates are also similar to those for carbonates exposed to aqueous fluids as

documented in Atkinson (1984). For the anhydrite caprocks (HB102, YB204), their fluid-weakening effect on K_{IC}^* and SCI is similar to that for carbonate caprocks. However, anhydrite caprocks have stronger water-weakening effects on K_{IC}^* , and water and formation water have similar effects (Fig. 5A and B). Among a few reported K_{IC} values for anhydrite/gypsum, our measured K_{IC}^* of 1.14 MPa $m^{1/2}$ for YB204 and 1.47 MPa $m^{1/2}$ for HB102 in air are larger than K_{IC} of ~ 1.07 MPa $m^{1/2}$ for gypsum rock (60%–85% gypsum) measured using Cracked Chevron Notched Brazilian Disc (CCNBD) specimens (Meng et al., 2015), which is consistent with the fact that anhydrite is macroscopically stronger than gypsum (Bell, 1981, 1994). Moreover, the high K_{IC}^* values of

$\sim 1.5 \text{ MPa m}^{1/2}$ for the purer anhydrite in HB102 in air is more than 4 times larger than theoretically calculated values of intergranular and grain boundary fractures for anhydrite crystal (Tromans and Meech, 2002), which is similar to observed stronger toughness in carbonate rocks than in single crystal calcite (Chen et al., 2019b). Except for the YB204, consistent K_{IC}^* and SCI dependency on fluid conditions are observed: air > formation water > water for K_{IC}^* (Fig. 5I–L), air > water > formation water for SCI (Fig. 5E–H). These observations provide insights into the mechanisms controlling fracture growth as will be discussed in the following section.

5.2. Fracture growth mechanisms

We now explore the possible mechanisms associated with our experimental observations. At ambient pressure/temperature conditions, calcite solubility increases with increasing water salinity (Mucci, 1983; Millero and Roy, 1997), while the anhydrite solubility increases first with water salinity then decreases at higher salt concentration (Klimchouk, 1996). The consistent SCI reduction from air to water toward formation water (Fig. 5E, G, 5H) can be linked to the mineral dissolution rates. Both anhydrite and calcite dissolve faster in saline water than in DI water. Existing data suggest that the faster the mineral dissolution rate, the lower the SCI (see Atkinson (1984) for carbonates and Chen et al. (2019a) for Marcellus Shale in HCl solution).

The consistent K_{IC}^* reduction from air to aqueous conditions for all the caprock samples is most likely resulted from the soaking process before the DT tests. Fracture toughness is a material property. As in the case of glass, the variation in fluid composition influences SCI through surficial processes such as stress-corrosion and dissolution reactions at the fracture surfaces, but K_{IC}^* , marking the initiation of critical crack growth in the material, is unaffected (Wiederhorn and Johnson, 1973). Indeed, the reduction in K_{IC}^* is linked to the physical weakening of the material in strength and elastic modulus, as in the case of water weakening in clay-bearing rocks (Nara et al., 2012; Chen et al., 2017, 2019a). The large surface area of the thin specimen slices (Fig. 3) enables more effective fluid-rock interaction than bulky samples. Anhydrite solubility is $\sim 2.5 \text{ g/L}$ in water at ambient condition, which is more than four orders of magnitude larger than calcite solubility of $\sim 1.5 \text{ mg/L}$ (Klimchouk, 1996). This explains why anhydrite caprocks have a stronger K_{IC}^* reduction than carbonate caprocks (Fig. 5A–D, 5I–5L). The stronger reduction in K_{IC}^* for anhydrite caprocks than carbonates is also in line with water-enhanced creep during salt deformation process (Urai et al., 1986). In addition, at ambient conditions, the irreversible anhydrite dissolution reaction can quickly transform anhydrite into gypsum with substantial volumetric expansion, which might also contribute to their larger K_{IC}^* reduction in solutions. The greater K_{IC}^* weakening in water than in formation water could not be explained by the dissolution rates since both anhydrite and calcite dissolve faster in saline water than in DI water. We suspect that the DI water with lower density can diffuse into the rock matrix more easily than the denser formation water, which causes stronger weakening effect.

It is not surprising that for both anhydrite and carbonate caprocks their K_{IC}^* values are much higher than their single-crystal counterparts because cracking multiple grain domains with different crystal orientations is harder than cracking a single crystal along the weak cleavage planes. The less preserved cleavage features along fracture surfaces of HB102 than YB204 (Fig. 7A–D) is likely due to faster dissolution reaction rates for smaller grains. Ambient humidity may also impact fresh anhydrite fracture surfaces, dissolving cleavage signatures (Fig. 7A). The lower K_{IC}^* for YB204 in air than HB102 indicates that multi-crystalline materials with smaller grain sizes are fracture mechanically stronger than those with bigger grains, most likely due to the diminished contribution of cleavage to fracture processes than rocks with larger grains. Grain size also influences fracture trace shapes. Fractures in multi-domain crystalline rocks have zigzag or step-like

shapes and wider damage zone (Fig. 7K) due to the combined effect of stress concentration (grooving and applied stress) and preferred cleavage planes, which can potentially provide more inter-crystal locking. Whereas fine-grain limestone is similar to a homogeneous material for fracture growth where individual grain has little influence on fracture trace (Fig. 7L).

5.3. Implications for reservoir sealing performance

Subsurface reservoirs need to meet certain seal performance in applications such as petroleum systems, carbon sequestration, and waste disposal. In general, anhydrite caprock is better than carbonate caprock, in its larger dry toughness (Fig. 5), lack of natural fractures (Fig. 7), and the strong ductility under subsurface stresses (Hangx et al., 2010). Although experimental opening-mode fractures have been generated for anhydrite under atmospheric pressure, the brittle-ductile transition under higher confining stresses and higher temperatures with increasing burial depth gradually suppresses brittle fracture growth as verified by the lack of natural fractures in anhydrite. Under higher confining stresses, brittle failure in anhydrite was taken over by plastic flow in the forms of grain boundary sliding, dislocation creeps, and solution transfer creep (Urai et al., 1986). One technical limitation of the current study is that the DT tests could only be performed under atmospheric stress instead of in-situ subsurface stress conditions (see method). Unlike rock mechanics tests, most fracture mechanical tests of rocks were performed without confining stresses (e.g., ISRM, 1988; Kuruppu et al., 2014). The reason is that the effective stress law controls fracture growth: fractures grow under positive driving stress, e.g., pore pressure P_p larger than minimum principal stress S_{hmin} for opening mode fractures. Even though our tests were performed under atmospheric pressure, our results can be applied to subsurface conditions where positive driving stresses exist, such as in scenarios with significant overpressure (large P_p with hydrocarbon accumulation) or tectonic uplift (small S_{hmin} active tectonics of the Himalaya orogeny). Indeed, the positive driving stress condition ($P_p > S_{hmin}$) does occur widely in nature as confirmed by the wide occurrence of opening-mode natural fractures in carbonate caprocks here (Fig. 6) and in other studies (Gale et al., 2014; Fall et al., 2015). Field data in the Sichuan Basin is a good example of evaporite caprock failure (Wang et al., 2013). Under subsurface pressure and temperature conditions, opening-mode fracturing through significant overpressure is the most likely failure mode to accommodate hydrocarbon loss for the evaporites. Once the reservoir pore pressure drops with hydrocarbon leakage, fractures within the evaporite caprock may heal/seal rapidly, and another cycle of over-pressurization - opening-mode failure - fracture heal/seal starts.

Temperature is another important parameter affecting rock failure processes. Though our current tests were not designed to investigate the temperature effect on fracture growth (all tests were at room temperature), studies have shown that higher temperature can have greater impact on subcritical fracture growth than fluid salinity and pH level variations (Atkinson, 1984; Chen et al., 2019a). In general, fractures grow faster and the rocks are weaker at higher temperatures due to enhanced physical and chemical interaction and reactions. However, caution should be made when applying the present results to higher temperature subsurface conditions with extreme cases such as the complex calcite dissolution kinetics (e.g., Naviaux et al., 2019).

Fluid chemistry is another main factor for fluid assisted fracture growth (Atkinson, 1984; Chen et al., 2019a), though not targeted in this study. Many fluid-rock interactions and reactions are functions of fluid chemistry such as the salinity-modulated clay hydration reactions (Chen et al., 2019a) and calcite dissolution reactions (Rostom et al., 2013), pH-adjusted quartz and calcite dissolution reactions (Wiederhorn and Johnson, 1973; Atkinson and Meredith, 1981; Chen et al., 2019a), to name a few. Oftentimes, the fluid chemistry and temperature act simultaneously in natural cases, making this problem even more complicated.

Our laboratory scale study focused on single fracture behavior under controlled fluid and temperature conditions. From the lab-scale single-crack case to the reservoir-scale cases with multiple interacting fractures, one need to perform upscaling geomechanical modeling that considers interactions among fracture mechanical properties (fracture network evolution, stress condition variation), hydrologic properties (transport properties evolutions), and fluid chemo-mechanical reactions (dissolution-precipitation, hydration, etc.) over relevant time scales. Nonetheless, experimental results demonstrate that aqueous fluids (water and formation water), rock composition (carbonate, anhydrite/gypsum), and rock texture (grain size) strongly influence fracture propagation for both carbonate and anhydrite caprocks, and the fluid composition effect is stronger for anhydrite caprocks. If aqueous fluids exist at the reservoir-caprock interface, the drying effect during the charging process in a gas reservoir like our case drives formation water away from the reservoir-caprock interface, which can potentially strengthen the caprocks at the reservoir-caprock interface. Another conclusion can be drawn from the different effects between water and formation water: caprocks have larger K_{IC}^* but smaller SCI in formation water (Fig. 5). This implies fracture growth in formation water is more difficult at high stress intensity factor (large K_{IC}^*) but easier under lower stress intensity factor (smaller SCI) than in water or low salinity solutions. Over short time scales such as during hydraulic fracturing operations (high stress), fracture growth in water is more natural. Nevertheless, over geologic time scales, faster subcritical fracture growth is expected in formation water environments.

6. Summary and conclusion

We conducted double torsion experiments at ambient conditions on carbonate and evaporite caprocks in Sichuan Basin, China, under environments of air, DI-water, and formation water to characterize the mechanical properties of fracture growth. The measured fracture toughness and SCI agree with test data from previous research. In ambient air, the anhydrite caprock (well HB102) has the largest fracture toughness of $1.47 \text{ MPa m}^{1/2}$, while the other three caprocks are weaker with toughness of $\sim 1.2 \text{ MPa m}^{1/2}$. Both fracture toughness and SCI of the caprocks are systematically reduced from ambient air condition to water environments: K_{IC}^* reduction is most active in the water, while SCI reduction is the strongest in formation water. The mechanical weakening process and microstructural observations suggest strong fluid-rock interactions (primarily dissolution reaction) during fracture growth. The larger dry toughness and lack of natural fractures suggest that anhydrite caprocks have better sealing performance in addition to its strong ductility under subsurface confine stress. Our results also suggest increased risk of fracture propagation in anhydrite caprocks than carbonates with the presence of saline fluids. This approach and data extend the mechanical evaluation of caprock integrity and improve the understanding of subcritical fracture growth.

CRedit authorship contribution statement

Zonghu Liao: Conceptualization, Methodology, Supervision, Writing - review & editing. **Mengni Wu:** Methodology, Writing - original draft, Writing - review & editing. **Xiaofeng Chen:** Conceptualization, Methodology, Supervision, Investigation, Writing - original draft, Writing - review & editing. **Huayao Zou:** Supervision, Writing - review & editing.

Declaration of competing interest

The authors declare that they have no known competing financial interests or personal relationships that could have appeared to influence the work reported in this paper.

Acknowledgments

The authors would like to thank Sinopec China for providing core samples. Support funds were provided by Strategic Priority Research Program of the Chinese Academy of Sciences XDA14010306, the National Natural Science Foundation of China (NSFC) No. 41604036 and NSFC Major Projects No. U1663203. Chen also acknowledges support from NSF grant EAR-1620330 "Investigating earthquake source processes in the laboratory". Assistance and discussions from Drs. Ze'ev Reches and Brett Carpenter during the visit of Mengni Wu at the University of Oklahoma are also greatly appreciated. Reviews from associate editor Friedemann Baur and two anonymous reviewers are appreciated that help improve our original paper.

Appendix A. Supplementary data

Supplementary data to this article can be found online at <https://doi.org/10.1016/j.marpetgeo.2020.104468>.

References

- Allan, U.S., 1989. Model for hydrocarbon migration and entrapment within faulted structures. *AAPG Bull.* 73 (7), 803–811. <https://doi.org/10.1306/44B4A271-170A-11D7-8645000102C1865D>.
- Anderson, T.L., 2005. *Fracture Mechanics: Fundamentals and Applications*. Taylor & Francis.
- Atkinson, B.K., 1982. Subcritical crack propagation in rocks: theory, experimental results and applications. *J. Struct. Geol.* 4 (1), 41–56. [https://doi.org/10.1016/0191-8141\(82\)90005-0](https://doi.org/10.1016/0191-8141(82)90005-0).
- Atkinson, B.K., 1984. Subcritical crack growth in geological materials. *J. Geophys. Res.: Solid Earth* 89 (B6), 4077–4114. <https://doi.org/10.1029/JB089iB06p04077>.
- Atkinson, B.K., Meredith, P.G., 1981. Stress corrosion cracking of quartz: a note on the influence of chemical environment. *Tectonophysics* 77, T1–T11. [https://doi.org/10.1016/0040-1951\(81\)90157-8](https://doi.org/10.1016/0040-1951(81)90157-8).
- Atkinson, B.K., Meredith, P.G., 1987. *Experimental Fracture Mechanics Data for Rocks and Minerals*. <https://doi.org/10.1016/B978-0-12-066266-1.50016-8>.
- Bell, F.G., 1981. Geotechnical properties of some evaporitic rocks. *Bull. Int. Assoc. Eng. Geol. Bull. Assoc. Internationale de Géologie de l'Ingénieur* 24 (1), 137–144. <https://doi.org/10.1007/BF02595264>.
- Bell, F.G., 1994. A survey of the engineering properties of some anhydrite and gypsum from the north and midlands of England. *Eng. Geol.* 38 (1–2), 1–23. [https://doi.org/10.1016/0013-7952\(94\)90021-3](https://doi.org/10.1016/0013-7952(94)90021-3).
- Bergsaker, A.S., Røyne, A., Ougier-Simonin, A., Aubry, J., Renard, F., 2016. The effect of fluid composition salinity, and acidity on subcritical crack growth in calcite crystals. *J. Geophys. Res.: Solid Earth* 121, 1631–1651. <https://doi.org/10.1002/2015JB012723>.
- Bildstein, O., Worden, R.H., Brosse, E., 2001. Assessment of anhydrite dissolution as the rate limiting step during thermochemical sulfate reduction. *Chem. Geol.* 176, 173–189. [https://doi.org/10.1016/S0009-2541\(00\)00398-3](https://doi.org/10.1016/S0009-2541(00)00398-3).
- Billi, A., Salvini, F., Storti, F., 2003. The damage zone-fault core transition in carbonate rocks: implications for fault growth, structure and permeability. *J. Struct. Geol.* 25 (11), 1779–1794. [https://doi.org/10.1016/S0191-8141\(03\)00037-3](https://doi.org/10.1016/S0191-8141(03)00037-3).
- Brantut, N., Heap, M.J., Meredith, P.G., Baud, P., 2013. Time-dependent cracking and brittle creep in crustal rocks: a review. *J. Struct. Geol.* 52, 17–43. <https://doi.org/10.1016/j.jsg.2013.03.007>.
- Callahan, O.A., Eichhubl, P., Olson, J.E., Davatzes, N.C., 2019. Fracture mechanical properties of damaged and hydrothermally altered rocks, dixie valley-stillwater fault zone, Nevada, USA. *J. Geophys. Res.: Solid Earth*. <https://doi.org/10.1029/2018JB016708>.
- Chen, X., Eichhubl, P., Olson, J.E., 2017. Effect of water on critical and subcritical fracture properties of Woodford shale. *J. Geophys. Res.: Solid Earth* 122 (4), 2736–2750. <https://doi.org/10.1002/2016JB013708>.
- Chen, X., Eichhubl, P., Olson, J.E., Dewers, T.A., 2019a. Salinity, pH, and temperature controls on fracture mechanical properties of three shales and their implications for fracture growth in chemically reactive fluid environments. *Geomechan. Energy Environ.* <https://doi.org/10.1016/j.gete.2019.100140>.
- Chen, X., Eichhubl, P., Olson, J.E., Dewers, T.A., 2019b. Effect of water on fracture mechanical properties of shales. *J. Geophys. Res.: Solid Earth* 124 (3), 2428–2444. <https://doi.org/10.1029/2018JB016479>.
- Chester, F.M., 1988. The brittle-ductile transition in a deformation-mechanism map for halite. *Tectonophysics* 154, 125–136. [https://doi.org/10.1016/0040-1951\(88\)90230-2](https://doi.org/10.1016/0040-1951(88)90230-2).
- Cipolla, C.L., Warpinski, N.R., Mayerhofer, M., Lolon, E.P., Vincent, M., 2010. The relationship between fracture complexity, reservoir properties, and fracture-treatment design. *SPE Prod. Oper.* 25 (4), 438–452. <https://doi.org/10.2118/115769-MS>.
- Cosgrove, J.W., 2001. Hydraulic fracturing during the formation and deformation of a basin: a factor in the dewatering of low-permeability sediments. *AAPG (Am. Assoc. Pet. Geol.) Bull.* 85 (4), 737–748. <https://doi.org/10.1306/8626C997-173B-11D7-8645000102C1865D>.

- Dai, J.X., Yu, C., Huang, S.P., Gong, D.Y., Wu, W., Fang, C.C., Liu, D., 2014. Geological and geochemical characteristics of large gas fields in China. *Petrol. Explor. Dev.* 41 (1), 1–13. [https://doi.org/10.1016/S1876-3804\(14\)60001-X](https://doi.org/10.1016/S1876-3804(14)60001-X).
- Deer, W.A., Howie, R.A., Zussmann, J., 1992. *An Introduction to the Rock-Forming Minerals*. Longman Scientific & Technical.
- Downey, M.W., 1984. Evaluating seals for hydrocarbon accumulations. *AAPG Bull.* 68 (11), 1752–1763.
- Erguler, Z.A., Ulusay, R., 2009. Water-induced variations in mechanical properties of clay-bearing rocks. *Int. J. Rock Mech. Min. Sci.* 46 (2), 355–370. <https://doi.org/10.1016/j.ijrmm.2008.07.002>.
- Fall, A., Eichhubl, P., Bodnar, R.J., Laubach, S.E., Davis, J.S., 2015. Natural hydraulic fracturing of tight-gas sandstone reservoirs. Piceance Basin, Colorado: GSA Bull. 127 (1–2), 61–75. <https://doi.org/10.1130/B31021.1>.
- Finkbeiner, T., Zoback, M., Flemings, P., Stump, B., 2001. Stress, pore pressure, and dynamically constrained hydrocarbon columns in the South Eugene Island 330 field, northern Gulf of Mexico. *AAPG (Am. Assoc. Pet. Geol.) Bull.* 85 (6), 1007–1031. <https://doi.org/10.1306/8626CA55-173B-11D7-8645000102C1865D>.
- Fisher, M., Normark, W., Bohannon, R., Sliter, R., Calvert, A., 2001. *Geology of the continental margin beneath Santa Monica Bay, southern California, from small-airgun, seismic-reflection data*. In: *AGU Fall Meeting Abstracts-1*, pp. 544.
- Fu, Y., Berk, W.V., Shulz, H.M., 2016. Hydrogen sulfide formation, fate, and behavior in anhydrite-sealed carbonate gas reservoirs: a three-dimensional reactive mass transport modeling approach. *AAPG (Am. Assoc. Pet. Geol.) Bull.* 100 (5), 843–865. <https://doi.org/10.1306/12111514206>.
- Fuller, E.R., 1979. An evaluation of double-torsion testing-analysis. *Fracture Mechanics Applied to Brittle Materials*. ASTM International, pp. 3–18. <https://doi.org/10.1520/STP36621S>.
- Fulljames, J.R., Zijerveld, L.J.J., Franssen, R.C.M.W., 1997. Fault seal processes: systematic analysis of fault seals over geological and production time scales. *Norwegian Petrol. Soc. Special Publ.* 7, 51–59. doi:10.1016/S0928-8937(97)80006-9.
- Gale, J.F., Laubach, S.E., Olson, J.E., Eichhubl, P., Fall, A., 2014. Natural fractures in shale: a review and new observations. *AAPG Bull.* 98 (11), 2165–2216. <https://doi.org/10.1306/08121413151>.
- Guo, T., 2018. Hydrocarbon accumulation conditions and key technologies for exploration and development of Yuanba gas field. *Petrol. Res.* 3 (4), 293–305. <https://doi.org/10.1016/j.ptlrs.2018.11.004>.
- Handin, J., Hager, R.V., 1958. Experimental deformation of sedimentary rocks under confining pressure: tests at high temperature. *AAPG Bull.* 42, 2892–2934. <https://doi.org/10.1306/OBDA5C27-16BD-11D7-8645000102C1865D>.
- Handin, J., Hager, R.V., Friedman, M., Feather, J.N., 1963. Experimental deformation of sedimentary rocks under confining pressure: pore pressure tests. *AAPG (Am. Assoc. Pet. Geol.) Bull.* 47, 717–755.
- Handin, J., Heard, H.C., Hagoquir, J.N., 1967. Effects of the intermediate principal stress on the failure of limestone, dolomite, and glass at different temperature and strain rates. *J. Geophys. Res.* 72, 611–640. <https://doi.org/10.1029/JZ072i002p00611>.
- Hangx, S.J., Spiers, C.J., Peach, C.J., 2010. Mechanical behavior of anhydrite caprock and implications for CO₂ sealing capacity. *J. Geophys. Res.: Solid Earth* 115. <https://doi.org/10.1029/2009JB006954>. B7.
- Hao, F., Zhu, W., Zou, H., Li, P., 2015. Factors controlling petroleum accumulation and leakage in overpressured reservoirs. *AAPG (Am. Assoc. Pet. Geol.) Bull.* 99 (5), 831–858. <https://doi.org/10.1306/01021514145>.
- Holder, J., Olson, J.E., Philip, Z., 2001. Experimental determination of subcritical crack growth parameters in sedimentary rock. *Geophys. Res. Lett.* 28 (4), 599–602. <https://doi.org/10.1029/2000GL011918>.
- Ingram, G.M., Urai, J.L., 1999. Top-seal leakage through faults and fractures: the role of mudrock properties. *Geol. Soc. Lond. Special Publ.* 158 (1), 125–135. <https://doi.org/10.1144/GSL.SP.1999.158.01.10>.
- ISRM, 1988. Suggested methods for determining the fracture toughness of rock. *Int. J. Rock Mech. Min. Geomechan. Abstract* 25, 71–96.
- Jin, X., Shah, S.N., Roggiers, J., Zhang, B., 2014a. Fracability evolution in shale reservoirs-an integrated petrophysical and geomechanics approach. *SPE, SPE-168589-MS*. <https://doi.org/10.2118/168589-MS>.
- Jin, Z., 2012. Formation and accumulation of oil and gas in marine carbonate sequences in Chinese sedimentary basins. *Sci. China Earth Sci.* 55 (3), 368–385. <https://doi.org/10.1007/s11430-011-4264-4>.
- Jin, Z., Yuan, Y., Sun, D., Liu, Q., Li, S., 2014b. Models for dynamic evaluation of mudstone/shale cap rocks and their applications in the lower Paleozoic sequences, Sichuan basin, SW China. *Mar. Petrol. Geol.* 49, 121–128. <https://doi.org/10.1016/j.marpetgeo.2013.10.001>.
- Klimchouk, A., 1996. The dissolution and conversion of gypsum and anhydrite. *Int. J. Speleol.* 25 (3–4), 21–36. <https://doi.org/10.5038/1827-806X.25.3.2>.
- Kuruppu, M.D., Obara, Y., Ayatollahi, M.R., Chong, K.P., Funatsu, T., 2014. ISRM suggested method for determining the mode I static fracture toughness using semi-circular bend specimen. *Rock Mech. Rock Eng.* 47, 267–274. <https://doi.org/10.1007/s00603-013-0422-7>.
- Lee, H.P., Olson, J.E., Holder, J., Gale, J.F., Myers, R.D., 2015. The interaction of propagating opening mode fractures with preexisting discontinuities in shale. *J. Geophys. Res.: Solid Earth* 120 (1), 169–181. <https://doi.org/10.1002/2014JB011358>.
- Li, P., Hao, F., Guo, X., Zou, H., Yu, X., Wang, G., 2015. Processes involved in the origin and accumulation of hydrocarbon gases in the Yuanba gas field, Sichuan Basin, southwest China. *Mar. Petrol. Geol.* 59, 150–165. <https://doi.org/10.1016/j.marpetgeo.2014.08.003>.
- Ma, Y., Guo, X., Guo, T., Huang, R., Cai, X., Li, G., 2007. The Puguang gas field: new giant discovery in the mature Sichuan Basin, southwest China. *AAPG Bull.* 91 (5), 627–643. <https://doi.org/10.1306/11030606062>.
- Ma, Y., Zhang, S., Guo, T., Zhu, G., Cai, X., Li, M., 2008. Petroleum geology of the Puguang sour gas field in the Sichuan Basin, SW China. *Mar. Petrol. Geol.* 25 (4–5), 357–370. <https://doi.org/10.1016/j.marpetgeo.2008.01.010>.
- Machel, H.G., 2001. Bacterial and thermochemical sulfate reduction in diagenetic settings-Old and new insights. *Sediment. Geol.* 140, 143–175. [https://doi.org/10.1016/S0037-0738\(00\)00176-7](https://doi.org/10.1016/S0037-0738(00)00176-7).
- Major, J.R., Eichhubl, P., Dewers, T.D., Olson, J.E., 2018. Effect of CO₂-brine-rock interaction on fracture mechanical properties of CO₂ reservoirs and seals. *Earth Planet. Sci. Lett.* 499, 37–47. <https://doi.org/10.1016/j.epsl.2018.07.013>.
- Meléndez-Martínez, J., Schmitt, D.R., 2016. A comparative study of the anisotropic dynamic and static elastic moduli of unconventional reservoir shales: implication for geomechanical investigations. *Geophysics* 81, D245–D261. <https://doi.org/10.1190/geo2015-0427.1>.
- Meng, T., Hu, Y., Fang, R., Kok, J., Fu, Q., Feng, G., 2015. Study of fracture toughness and weakening mechanisms in gypsum interlayers in corrosive environments. *J. Nat. Gas Sci. Eng.* 26, 356–366. <https://doi.org/10.1016/j.jngse.2015.06.027>.
- Meredith, P.G., Atkinson, B.K., 1985. Fracture toughness and subcritical crack growth during high-temperature tensile deformation of Westerly granite and Black gabbro. *Phys. Earth Planet. In.* 39 (1), 33–51. [https://doi.org/10.1016/0031-9201\(85\)90113-X](https://doi.org/10.1016/0031-9201(85)90113-X).
- Millero, F.J., Roy, R.N., 1997. A chemical equilibrium model for the carbonate system in natural waters. *Croat. Chem. Acta* 70 (1), 1–38.
- Mucci, A., 1983. The solubility of calcite and aragonite in seawater at various salinities, temperatures, and one atmosphere total pressure. *Am. J. Sci.* 283 (7), 780–799. <https://doi.org/10.2475/ajs.283.7.780>.
- Nara, Y., Kaneko, K., 2006. Sub-critical crack growth in anisotropic rock. *Int. J. Rock Mech. Min. Sci.* 43, 437–453. <https://doi.org/10.1016/j.ijrmm.2005.07.008>.
- Nara, Y., Morimoto, K., Hiro Yoshi, N., Yoneda, T., Kaneko, K., Benson, P.M., 2012. Influence of relative humidity on fracture toughness of rock: implications for sub-critical crack growth. *Int. J. Solid Struct.* 49 (18), 2471–2481. <https://doi.org/10.1016/j.ijsols.2012.05.009>.
- Naviaux, J.D., Subhas, A.V., Rollings, N.E., Dong, S., Berelson, W.M., Adkins, J.F., 2019. Temperature dependence of calcite dissolution kinetics in seawater. *Geochem. Cosmochim. Acta* 246, 363–384. <https://doi.org/10.1016/j.gca.2018.11.037>.
- Olson, J.E., 1993. Joint pattern development: effects of subcritical crack growth and mechanical crack interaction. *J. Geophys. Res.: Solid Earth* 98 (B7), 12251–12265. <https://doi.org/10.1029/93JB00779>.
- Olson, J.E., Laubach, S.E., Lander, R.H., 2009. Natural fracture characterization in tight gas sandstones: integrating mechanics and diagenesis. *AAPG Bull.* 93 (11), 1535–1549. <https://doi.org/10.1306/08110909100>.
- Piane, C.D., Clennell, M.B., Keller, J.V.A., Giwelli, A., Luzin, V., 2017. Carbonate hosted fault rocks: a review of structural and microstructural characteristic with implications for seismicity in the upper crust. *J. Struct. Geol.* 103, 17–36. <https://doi.org/10.1016/j.jsg.2017.09.003>.
- Reches, Z., Lockner, D.A., 1994. Nucleation and growth of faults in brittle rocks. *J. Geophys. Res.* 99 (B9), 18159–18173. <https://doi.org/10.1029/94JB00115>.
- Renner, J., Rummel, F., 1996. The effect of experimental and microstructural parameters on the transition from brittle failure to cataclastic flow of carbonate rock. *Tectonophysics* 258, 151–169. [https://doi.org/10.1016/0040-1951\(95\)00192-1](https://doi.org/10.1016/0040-1951(95)00192-1).
- Rostom, F., Royné, A., Dysthe, D.K., Renard, F., 2013. Effect of fluid salinity on subcritical crack propagation in calcite. *Tectonophysics* 583, 68–75. <https://doi.org/10.1016/j.tecto.2012.10.023>.
- Shimamoto, T., 1986. Transition between frictional slip and ductile flow for halite shear zones at room temperature. *Science* 231, 711–714. <https://doi.org/10.1126/science.231.4739.711>.
- Smith, D.A., 1966. Theoretical considerations of sealing and non-sealing faults. *AAPG (Am. Assoc. Pet. Geol.) Bull.* 50 (2), 363–374. <https://doi.org/10.1306/5D25B48F-16C1-11D7-8645000102C1865D>.
- Sone, H., Zoback, M.D., 2013. Mechanical properties of shale-gas reservoirs-Part 2: ductile creep, brittle strength, and their relation to the elastic modulus. *Geophysics* 78 (5), 393–402. <https://doi.org/10.1190/geo2013-0051.1>.
- Swanson, P.L., 1984. Subcritical crack growth and other time- and environment-dependent behavior in crustal rocks. *J. Geophys. Res.: Solid Earth* 89 (B6), 4137–4152. <https://doi.org/10.1029/JB089i06p04137>.
- Tingay, M.R.P., Hillis, R.R., Swarbrick, R.E., Morley, C.K., Damit, A.R., 2009. Origin of overpressure and pore-pressure prediction in the Baram province, Brunei. *AAPG (Am. Assoc. Pet. Geol.) Bull.* 93 (1), 51–74. <https://doi.org/10.1306/08080808016>.
- Tromans, D., Meech, J.A., 2002. Fracture toughness and surface energies of minerals: theoretical estimates for oxides, sulphides, silicates and halides. *Miner. Eng.* 15 (12), 1027–1041. [https://doi.org/10.1016/S0892-6875\(02\)00213-3](https://doi.org/10.1016/S0892-6875(02)00213-3).
- Urai, J.L., Spiers, C.J., Zwart, H.J., Lister, G.S., 1986. Weakening of rock salt by water during long-term creep. *Nature* 324 (6097), 554–557. <https://doi.org/10.1038/324554a0>.
- Wang, Z., Huang, S., Gong, D., Wu, W., Yu, C., 2013. Geochemical characteristics of natural gases in the upper triassic Xujiahe formation in the southern Sichuan Basin, SW China. *Int. J. Coal Geol.* 120, 15–23. <https://doi.org/10.1016/j.coal.2013.09.002>.
- Watts, N.L., 1987. Theoretical aspects of cap-rock and fault seals for single- and two-phase hydrocarbon columns. *Mar. Petrol. Geol.* 4 (4), 274–307. [https://doi.org/10.1016/0264-8172\(87\)90008-0](https://doi.org/10.1016/0264-8172(87)90008-0).
- Wei, S., Feng, Q., Feng, Y., Yuan, S., 2011. Prediction of triassic gypsum cap rocks in Tongnanba region of Northeast Sichuan basin. *Petrol. Geol. Exp.* 33 (1), 81–86 (In Chinese).
- Wiederhorn, S.M., Johnson, H., 1973. Effect of electrolyte pH on crack propagation in glass. *J. Am. Ceram. Soc.* 56 (4), 192–197. <https://doi.org/10.1111/j.1151-2916.1973.tb12454.x>.

- Williams, D.P., Evans, A.G., 1973. A simple method for studying slow crack growth. *J. Test. Eval.* 1 (4), 264–270. <https://doi.org/10.1520/JTE10015J>.
- Yielding, G., Freeman, B., Needham, D.T., 1997. Quantitative fault seal prediction. *AAPG Bull.* 81 (6), 897–917.
- Zhang, X., Lu, Y., Tang, J., Zhou, Z., Liao, Y., 2017. Experimental study on fracture initiation and propagation in shale using supercritical carbon dioxide fracturing. *Fuel* 190, 370–378. <https://doi.org/10.1016/j.fuel.2016.10.120>.
- Zhang, Y., Lu, H., Hu, H., 2012. Distribution of gypsum-salt cap rocks in Yuanba area of northeastern Sichuan Basin. *Xingjiang Petrol. Geol.* 33 (4), 450–452 (In Chinese).
- Zoback, M., 2010. *Reservoir Geomechanics*. Cambridge University Press.